Journal of Nonlinear Modeling and Analysis
Volume 7, Number 5, October 2025, 1611–1641
https://journal.global-sci.org/jnma
DOI:10.12150/jnma.2025.1611

Haar Wavelet Operational Matrix Approach for the Numerical Solution of Fractional Order Diabetes Mellitus Model

S. Kumbinarasaiah[1,†] and R. Yeshwanth[1]

Abstract Diabetes is a chronic disease which many people suffer from seriously. This study introduces a novel approach called the Haar wavelet collocation method (HWCM) to study the analysis and numerical approximation of the fractional order diabetes mellitus model. We built the operational matrix of integration (OMI) using the Haar wavelet to solve the diabetes mellitus model, a system of fractional differential equations. First, we transform the diabetes mellitus model into a system of algebraic equations using the operational matrix of integration of the Haar wavelet. The obtained system is further considered using the Newton-Raphson technique to extract the unknown Haar coefficients. Here, we use the calculus of fractional derivatives of a mathematical model to study and investigate the dynamic behavior of diabetes. We find numerical results for the validation of fractional order derivatives. Using the model parameter values, these numerical results are seen from both mathematical and biological perspectives. Numerical tables and graphical representations provide a visual presentation of the obtained results. The results of the developed method, the RK4 method, and the ND solver solution are compared. The numerical results show how highly accurate and efficient HWCM is in solving the fractional order diabetes mellitus model. Further, we show the method's efficacy and dynamics in various settings by performing simulations with parameter values. Mathematica, a mathematical software, has been utilized for numerical computations and implementation.

Keywords Caputo fractional derivative, collocation method, operational matrix of integration, Haar wavelet, fractional order diabetes mellitus model

MSC(2010) 34B16, 34A12, 65L05, 65T60, 68Q07.

1. Introduction

Chronic metabolic diseases like diabetes mellitus continue to pose a serious threat to world health. It is a long-term metabolic disorder defined by persistently high blood glucose levels brought on by insulin production action insufficiencies or both. These abnormalities disrupt the metabolism of proteins, fats, and carbohydrates, highlighting the pivotal role of insulin as an anabolic hormone. Patients with diabetes have a higher risk of coronary artery disease and are four times more likely

[†]the corresponding author.
Email address:kumbinarasaiah@gmail.com(Kumbinarasaiah S.), yeshuysr@gmail.com(Yeshwanth R.)
[1]Department of Mathematics, Bangalore University, Bengaluru, India.

to have a stroke compared to individuals without the condition. Untreated diabetes poses several risks, including abnormalities in vision that can result in blindness, increased susceptibility to infections, and loss of consciousness. On the other hand, some people, especially kids with total insulin deficiency, might exhibit obvious symptoms like polyuria (excessive urination), polydipsia (excessive thirst), polyphagia (increased appetite), blurred vision, and unintentional weight loss. The International Diabetes Federation estimates that by 2040, there will be an additional 200 million people with diabetes mellitus worldwide from the approximately 415 million who had the condition in 2015 [1]. A wide range of genetic susceptibilities, including differences in genes related to insulin secretion, production, and regulation, are included in the etiology of diabetes mellitus. Diabetes mellitus is characterized by intricate disruptions in protein homeostasis, lipid metabolism, and glucose metabolism. Vast research efforts have been devoted to determining the etiology of diabetes mellitus, investigating the underlying pathophysiological mechanisms, and creating efficient treatment approaches as our understanding of the condition grows [7].

To find cures for the epidemics and plagues that have beset humanity, infectious disease modeling has attracted a lot of attention recently. In the literature, integer-order infection models have been the subject of numerous studies. Omame et al. [6], highlighted the importance of taking preventative measures for COVID-19 and Dengue co-infection in Brazil using an integer order model. An integer-order co-infection model of Dengue fever, Zika virus cholera and Buruli ulcer, syphilis, and HPV with optimal control was the main focus of the authors [3–6]. But the models listed above have drawbacks because they don't account for memory, an essential component of faithfully simulating real-world situations [2].

This article aims to present a mathematical formulation of the diabetes mellitus model, which has attracted significant attention from the scientific community. In the mathematical modeling of diabetes mellitus, blood glucose, insulin, and other relevant variables are modeled mathematically to understand and explain their dynamics. These models are useful for researching the illness's fundamental causes, evaluating different treatment approaches, and modeling its course. Diabetes mathematical models are helpful for research and clinical applications. They aid in comprehending the illness and provide direction for creating more potent treatment regimens.

Consider the following diabetes mellitus disease mathematical model in the form of a system of ordinary differential equations [8]:

$$\left.\begin{aligned} \tfrac{d\mathcal{S}(t)}{dt} &= \gamma - \rho\mathcal{S} - \chi\mathcal{I} - \mu\mathcal{R}, \\ \tfrac{d\mathcal{X}(t)}{dt} &= \eta(\mathcal{S} - \mathcal{X} - \mathcal{I} - \mathcal{R})\mathcal{X} - (\rho+1)\mathcal{X}, \\ \tfrac{d\mathcal{I}(t)}{dt} &= \varepsilon\nu\mathcal{X} - (\rho+\chi)\mathcal{I}, \\ \tfrac{d\mathcal{R}(t)}{dt} &= (1-\varepsilon\nu)\mathcal{X} - (\rho+\mu)\mathcal{R}, \end{aligned}\right\} \tag{1.1}$$

with the initial conditions: $\mathcal{S} = \mathcal{S}_0$, $\mathcal{X} = \mathcal{X}_0$, $\mathcal{I} = \mathcal{I}_0$, $\mathcal{R} = \mathcal{R}_0$.

The above set of non-linear equations is used to describe this complex model. This diabetes model is divided into four subclasses: susceptible individuals $\mathcal{S}(t)$, carrier infectious individuals $\mathcal{X}(t)$, infectious individuals $\mathcal{I}(t)$, recovered individuals $\mathcal{R}(t)$ and environmental bacteria concentration $\mathcal{N}(t)$=$\mathcal{S}(t)$+$\mathcal{X}(t)$+$\mathcal{I}(t)$+$\mathcal{R}(t)$ denotes the total population number at time t. The model parameters are as follows:

γ represents births in a given time range; ρ represents deaths in a given time range; χ represents disease-specific fatality rate; μ represents disease-related mortality rate with treatment; $\varepsilon\nu$ represents the rate of transmission from latent to infected individuals without treatment; η represents the rate of transmission from susceptible to exposed individuals.

A fractional differential equation (FDE) is a type of mathematical equation that extends the idea of differentiation to non-integer values and deals with derivatives of non-integer orders or fractions. FDEs, which describe complex systems with memory, long-range dependence, and non-local effects, involve fractional derivatives instead of ordinary differential equations (ODEs), where derivatives are of integer orders. Many scientific disciplines have recently shown great interest in fractional differential equations because they provide a solid foundation for modeling and understanding complex systems with long-range dependencies and memory effects. Here, we look at the system of nonlinear differential equations using the Caputo fractional operator of order α, where $\alpha \in (0, 1]$.

$$\left.\begin{aligned} \frac{d_t^\alpha \mathcal{S}(t)}{dt} &= \gamma - \rho\mathcal{S} - \chi\mathcal{I} - \mu\mathcal{R}, \\ \frac{d_t^\alpha \mathcal{X}(t)}{dt} &= \eta(\mathcal{S} - \mathcal{X} - \mathcal{I} - \mathcal{R})\mathcal{X} - (\rho + 1)\mathcal{X}, \\ \frac{d_t^\alpha \mathcal{I}(t)}{dt} &= \varepsilon\nu\mathcal{X} - (\rho + \chi)\mathcal{I}, \\ \frac{d_t^\alpha \mathcal{R}(t)}{dt} &= (1 - \varepsilon\nu)\mathcal{X} - (\rho + \mu)\mathcal{R}. \end{aligned}\right\} \tag{1.2}$$

This model has been studied by numerous researchers, including the Caputo Fabrizio fractional order model for glucose control in insulin therapies for diabetes [9], the fractional-order mathematical model of diabetes and the complications that result from it [10], the effect of an awareness program on diabetes mellitus as described by the fractional-order model solved by homotopy analysis method [11], stability analysis for the nabla discrete fractional-order of the glucose-insulin regulating system on diabetes mellitus with a Mittag-Leffler kernel [12], fractional order PID controller for diabetes patients [13], and the glucose-insulin regulatory system on diabetes mellitus [14, 15].

Joseph Fourier discovered in the early 1800s that sines and cosines could be used to express a variety of functions, which is regarded as a significant advance in mathematical analysis. Techniques for superposing distinct functions to approximate other functions were developed due to this discovery. Despite their essential contribution to the development of Fourier analysis, sines and cosines are not well adapted for estimating noisy signals. Mathematicians have, therefore, been searching for more effective ways to approximate these signals. It should be mentioned that these functions have infinite extensions because they are non-local. As a result, they can't accurately represent acute spikes.

Wavelet analysis, however, offers a good substitute for Fourier analysis since it can approximate functions precisely confined to finite domains. Various signals with abrupt discontinuities or sharp spikes can be approximated using wavelets, functions with finite support. Considering how commonplace these discontinuities are in real-world communications, wavelets' capacity to manage them is especially important. Wavelet analysis is crucial in numerous practical applications, such as data analysis, signal compression, and picture processing. Furthermore, waves have been used in various disciplines, including geology, physics, and finance. Therefore, recent research has focused on wavelet-based numerical approaches because

they are efficient. During the last two decades, wavelets have made a great deal of progress in terms of their application. There are several wavelets to study the differential equations, such as the numerical solution of differential equations using Haar wavelets [16], Haar wavelet transform for integral and differential equations [17], Haar wavelet technique to study Chlamydia transmission [18], Hermite wavelet technique to study the squeezing flow in Casson fluid [19], the study of nonlinear fractional Klein-Gordan equation [20], numerical solution of time-fractional telegraph equations [21], numerical solution of SEIR epidemic model of measles and smoking using Fibonacci wavelets [22], numerical solution of stiff systems in chemistry using Taylor wavelet collocation method [23], the study of economic and environmental mathematical model [24], biological pest model in Tea plants using Haar wavelet [25], Haar wavelet method for fractional advection diffusion equations [26], Fibonacci wavelet method for convection diffusion equation [27], evolution of smoking habit model through Haar wavelet method [28], marriage divorce mathematical model [29], Taylor wavelet method for tumor growth model [30], Gegenbauer wavelets method for electrical circuits model [31], wavelets collocation method for perturbed differential difference equations [32] .

Haar wavelets are useful for numerical techniques in several applications, such as function approximation and differential equation solutions. The HWCM can sometimes provide several benefits, even if many sophisticated numerical methods are available for these tasks. This approach might be significant for the following reasons:

High Accuracy: The HWCM can provide high-accuracy approximations of functions and solutions to differential equations. The use of Haar wavelets can represent complex functions with high precision, even in areas of rapid change.

Efficiency: The HWCM can be computationally efficient when solving problems with smooth solutions. Collocation techniques reduce computing times and utilize less memory, avoiding large matrix operations.

Flexibility: The HWCM can solve a wide range of problems, including those with irregular domains and boundary conditions. This flexibility can be especially helpful in applications like signal analysis and image processing, where complex data sets may call for unique solution techniques.

Wavelet Analysis: This method's usage of Haar wavelets enables wavelet analysis of the solution, revealing information about the solution's various characteristics and frequency content. This can be especially helpful when detecting and isolating significant features, like signal processing, which is crucial.

The HWCM can offer unique benefits in specific circumstances, even if several sophisticated numerical methods are accessible. This approach is the best choice for applications requiring the highest levels of precision, effectiveness, adaptability, and wavelet analysis capabilities. It is an excellent option for specialist fields like signal processing, image analysis, and others that call for exact approximations and unique solutions. This approach stands out due to its superior capabilities, delivering unmatched performance. This approach is an ideal tool that you can depend on to yield the best outcomes while analyzing intricate data sets or making accurate estimations.

This paper is organized as follows. Section 2, named "Preliminaries," defines Caputo fractional derivatives, Haar wavelets, and OMI of Haar wavelets. Section 3 demonstrates its convergence analysis theorem. Section 4 proposes the solution for integer and fractional order, and Section 5 presents a discussion of numerical

results. Finally, Section 6 concludes the article.

2. Preliminaries of fractional derivative and Haar wavelets

Definition 2.1. The Riemann-Liouville's fractional integral of $g \in C_\mu$ of the order $\delta \geq 0$ defined as [36],

$$J_s^\delta g(s) = \begin{cases} g(s) & if \quad \delta = 0, \\ \frac{1}{\Gamma(\delta)} \int_0^s (s-t)^{\delta-1} g(t) dt & if \quad \delta > 0. \end{cases}$$

The gamma function is indicated here by the symbol Γ, where C_μ is a continuous linear space.

Definition 2.2. The Caputo fractional derivative of $g(s) \in C_\mu$ is defined as [36]:

$$\frac{\partial^\delta g(s)}{\partial s^\delta} = \frac{1}{\Gamma(p-\delta)} \int_0^s (s-t)^{p-\delta-1} g^{(p)}(t) dt$$

for $p-1 < \delta \leq p$, p is any positive integer, $s > 0$, and $g(s) \in C_\mu^p, \mu \geq -1$, where C_μ^p is a continuous linear space containing $g^p(s)$.

Definition 2.3. A wavelet $\psi(t)$ is a real function with the conditions:

$$\int_{-\infty}^{\infty} \psi(t)\, dt = 0 \qquad \text{and} \qquad \int_{-\infty}^{\infty} |\psi(t)|^2 dt = 1.$$

$\psi(t)$ must satisfy the first criterion, which requires it to be a periodic function with zero mean, and the other one, which guarantees unit energy. To be more exact, wavelets are described as,

$$\psi_{a,b}(t) = \tfrac{1}{\sqrt{a}} \psi(\tfrac{t-b}{a}), \ b, a \neq 0 \in \mathbb{R}.$$

Here, the translation parameter is b, and the dilation parameter is a.

2.1. OMI of integer order

A subset $[a, b]$ of $\mathbb{R}$ is partitioned into equal-length 2M sub-intervals, where each sub-interval has a length of $\Delta t = \frac{(b-a)}{2M}$, and $M = 2^J$, with J being the maximal level of resolution. We consider two parameters: $k = 0, 1, ..., m-1$, and $j = 0, 1, 2, ..., J$, where $m = 2^j$. The wavelet number $i = m + k + 1$, where k is the translation, and j is the dilation parameter. Next, we define the i^{th} Haar wavelet as

$$h_i(t) = \begin{cases} 1, & for \quad t \in [\zeta_1(i), \zeta_2(i)), \\ -1, & for \quad t \in [\zeta_2(i), \zeta_3(i)), \\ 0, & otherwise, \end{cases} \tag{2.1}$$

where,

$$\zeta_1(i) = a + 2k\Lambda\Delta t, \tag{2.2}$$
$$\zeta_2(i) = a + (2k+1)\Lambda\Delta t, \tag{2.3}$$
$$\zeta_3(i) = a + 2\,(k+1)\Lambda\Delta t, \tag{2.4}$$

$$\Lambda = \frac{M}{m}. \tag{2.5}$$

(2.1) is true when $i > 1$. If $i = 1$, we have,

$$h_1(t) = \begin{cases} 1, & for \quad t \in [a, b), \\ 0, & otherwise. \end{cases} \tag{2.6}$$

(2.6) is known as the Haar scalar function. The OMI is,

$$p_{\beta,i}(t) = \underbrace{\int_a^t \int_a^t \int_a^t ... \int_a^t}_{\beta \text{ times}} h_i(t) dt^{\beta}, \tag{2.7}$$

where, $\beta = 1, ..., n,\ i = 1, ..., 2M$. And if $i = 1$, we have

$$p_{\beta,1}(t) = \frac{1}{\beta!} (t - a)^{\beta}. \tag{2.8}$$

For $i \geq 2$, we have

$$p_{\beta,i}(t) = \begin{cases} 0, & for \quad t < \zeta_1(i), \\ \frac{1}{\beta!}[t - \zeta_1(i)]^{\beta}, & for \quad t \in [\zeta_1(i), \zeta_2(i)], \\ \frac{1}{\beta!}\{[t - \zeta_1(i)]^{\beta} - 2[t - \zeta_2(i)]^{\beta}\}, & for \quad t \in [\zeta_2(i), \zeta_3(i)], \\ \frac{1}{\beta!}\{[t - \zeta_1(i)]^{\beta} - 2[t - \zeta_2(i)]^{\beta} + [t - \zeta_3(i)]^{\beta}\}, & for \quad t > \zeta_3(i). \end{cases} \tag{2.9}$$

For $J = 2$, the OMI is as follows:

$$p_{1,i} = \begin{bmatrix} 0.0625 & 0.1875 & 0.3125 & 0.4375 & 0.5625 & 0.6875 & 0.8125 & 0.9375 \\ 0.0625 & 0.1875 & 0.3125 & 0..4375 & 0.4375 & 0.3125 & 0.1875 & 0.0625 \\ 0.0625 & 0.1875 & 0.1875 & 0.0625 & 0 & 0 & 0 & 0 \\ 0 & 0 & 0 & 0 & 0.0625 & 0.1875 & 0.1875 & 0.0625 \\ 0.0625 & 0.0625 & 0 & 0 & 0 & 0 & 0 & 0 \\ 0 & 0 & 0.0625 & 0.0625 & 0 & 0 & 0 & 0 \\ 0 & 0 & 0 & 0 & 0.0625 & 0.0625 & 0 & 0 \\ 0 & 0 & 0 & 0 & 0 & 0 & 0.0625 & 0.0625 \end{bmatrix}.$$

2.2. OMI of fractional order

Consider a subset [A, B] $\subset \mathbb{R}$ partitioned into m sub-intervals, each of width $\Delta x = \frac{B-A}{m}$. Given an interval [A, B], the i^{th} orthogonal set of Haar wavelets is as follows:

$$h_i(x) = \begin{cases} 1, & \zeta_1(i) \leq x < \zeta_2(i), \\ -1, & \zeta_2(i) \leq x < \zeta_3(i), \\ 0, & otherwise. \end{cases} \tag{2.10}$$

Here,

$$\begin{aligned}\zeta_1(i) &= A + \frac{k-1}{2^j} m\Delta x,\\ \zeta_2(i) &= A + \frac{k-(\frac{1}{2})}{2^j} m\Delta x,\\ \zeta_3(i) &= A + \frac{k}{2^j} m\Delta x,\end{aligned}$$

where J is a positive integer and $i = 1, 2, ..., m = 2^J$, and m is the greatest level of resolution. In this case, the decomposition of the integer index i is represented by j and k, where $i = 2^j + k - 1$, $0 \le j < 1$, and $1 \le k < 2^j + 1$. For $i \ge 2$, equation (2.10) holds true; for $i = 1$, we have,

$$h_i(x) = \begin{cases} 1, & for \quad x \in [A, B], \\ 0, & otherwise. \end{cases} \tag{2.11}$$

The Haar wavelet OMI $Q^\alpha H_m(x)$ of order α is,

$$Q^\alpha H_m(x) = [Qh_0(x), Qh_1(x), Qh_2(x), ..., Qh_{m-1}(x)]^T, \tag{2.12}$$

where,

$$Qh_i(x) = \begin{cases} 0, & A \le x < \zeta_1(i), \\ \Phi_1, & \zeta_1(i) \le x < \zeta_2(i), \\ \Phi_2, & \zeta_2(i) \le x < \zeta_3(i), \\ \Phi_3, & \zeta_3(i) \le x < B, \end{cases} \tag{2.13}$$

and

$$\begin{aligned}\Phi_1 &= \frac{(x-\zeta_1(i))^\alpha}{\Gamma(\alpha+1)},\\ \Phi_2 &= \frac{(x-\zeta_1(i))^\alpha}{\Gamma(\alpha+1)} - 2\frac{(x-\zeta_2(i))^\alpha}{\Gamma(\alpha+1)},\\ \Phi_3 &= \frac{(x-\zeta_1(i))^\alpha}{\Gamma(\alpha+1)} - 2\frac{(x-\zeta_2(i))^\alpha}{\Gamma(\alpha+1)} + \frac{(x-\zeta_3(i))^\alpha}{\Gamma(\alpha+1)}.\end{aligned}$$

Equation (2.13) holds true for $i \ge 1$. If $i = 0$, we have

$$Qh_0(x) = \begin{cases} \frac{x^\alpha}{\Gamma(\alpha+1)}, & x \in [A, B], \\ 0, & otherwise. \end{cases}$$

When α is fractional, for example, we have

For $J = 3$, $\alpha = 0.4$.

$$Q^{1-\alpha}H_m(x) = Q^{0.6}H_m(x) = \begin{bmatrix} 0.21204 & 0.40992 & 0.55693 & 0.68153 & 0.79244 & 0.89384 & 0.98808 & 1.07667 \\ 0.21204 & 0.40992 & 0.55693 & 0.68153 & 0.36836 & 0.07400 & -0.12579 & -0.28639 \\ 0.21204 & 0.40992 & 0.13285 & -0.13831 & -0.10938 & -0.05929 & -0.03987 & -0.02949 \\ 0 & 0 & 0 & 0 & 0.21204 & 0.40992 & 0.13285 & -0.13831 \\ 0.21204 & -0.01416 & -0.05085 & -0.02242 & -0.01367 & -0.00952 & -0.00715 & -0.00565 \\ 0 & 0 & 0.21204 & -0.01416 & -0.05085 & -0.02242 & -0.01367 & -0.00952 \\ 0 & 0 & 0 & 0 & 0.21204 & -0.01416 & -0.05085 & -0.02242 \\ 0 & 0 & 0 & 0 & 0 & 0 & 0.21204 & -0.014168 \end{bmatrix}.$$

Similarly, for various values of α, we can produce the OMI of Haar wavelets according to our needs.

3. Some results on the Haar wavelets

Let i, j be integers and the Haar function $\psi_{i,j}$ be characterised as, $\psi_{i,j}(x) = 2^{\frac{i}{2}}\psi(2^i x - j)$, $\forall x \in \mathbb{R}$ be endorsed on $\left[\frac{j}{2^i}, \frac{(j+1)}{2^i}\right)$ with the property $\int\limits_{\mathbb{R}} \psi_{i,j}(x)dx = 0$ and $||\psi_{i,j}||_2^2 = \int\limits_{\mathbb{R}} \psi_{i,j}^2(x)dx = 1$.

Theorem 3.1. *Let $\{\psi_{i,j}(t)|i, j \in \mathbb{Z}\}$ be a set of the Haar wavelets on $\mathbb{R}$. Then, the space $L^2(\mathbb{R})$ generated by Haar wavelets is complete.*

Proof. Consider that $\{\psi_{i,j}(t)|i, j \in \mathbb{Z}\}$ is spans the $L^2(\mathbb{R})$ called normed linear space. The cauchy sequence $\{\psi_{i,j}^k\}$ in $L^2(\mathbb{R})$ is defined as follows: for a given $\epsilon = \frac{1}{2} > 0$, there exists a positive integer $\eta_1 \ni : ||\psi_{i,j}^k - \psi_{i,j}^l||_2 < \frac{1}{2},\ \forall k, l \geq \eta_1$.
For $\epsilon = \frac{1}{2}$, choose $\psi_{i,j}^{k_1}$, such that $||\psi_{i,j}^{k_1} - \psi_{i,j}^{k_2}||_2 < \frac{1}{2}$, $\forall k_1, k_2 \geq \eta_1$;
For $\epsilon = \frac{1}{2^2}$, choose $\psi_{i,j}^{k_2}$, such that $||\psi_{i,j}^{k_2} - \psi_{i,j}^{k_3}||_2 < \frac{1}{2^2}, \forall k_2, k_3 \geq \eta_2$;

$$\vdots$$

For $\epsilon = \frac{1}{2^n}$, choose $\psi_{i,j}^{k_n}$ such that $||\psi_{i,j}^{k_n} - \psi_{i,j}^{k_{n+1}}||_2 < \frac{1}{2^n},\ \forall k_n, k_{n+1} \geq \eta_n$.

Therefore, $\{\psi_{i,j}^{k_n}\}$ is a sub-sequence of $\{\psi_{i,j}^k\}$. It shows that, $\sum\limits_{k=1}^{\infty} ||\psi_{i,j}^{k_{n+1}} - \psi_{i,j}^{k_n}||_2 \leq \sum\limits_{n=1}^{\infty} \frac{1}{2^n} = 1$.

Consider, $\phi_n = |\psi_{k_1}| + |\psi_{k_2} - \psi_{k_1}| + ... + |\psi_{k_{n+1}} - \psi_{k_n}|$, for $n = 1, 2, ...$
$\implies$ the sequence $\{\phi_n\}$ is the non-negative increasing measurable functions, therefore,
$||\phi_n||_2^2 = [||\psi_{k_1}||_2 + \sum\limits_1 ||\psi_{k_{n+1}} - \psi_{k_n}||_2]^2$, (by Minkowski inequality)
$||\phi_n||_2^2 \leq (||\psi_{k_1}||_2 + 1)^2 < \infty$.

Consequently ϕ_n is an increasing and bounded sequence, and there exists ϕ such that $\lim\limits_{n\to\infty} \phi_n = \phi$. By the theorem of monotone convergence, we have $\int \phi^2 dx = \lim\limits_{n\to\infty} \int \phi_n^2 dx < \infty \implies \phi \in L_p(\mathbb{R})$.

$\implies$ The series $\psi_{k_1}(x) + \sum\limits_1^{\infty} |\psi_{k_{n+1}}(x) - \psi_{k_n}(x)|$ converges almost eveywhere so that $\forall x \in A$, $\{\psi_{k_n}\}$ converges to $\psi(x)$, where A is a measurable set.

Again, let $\epsilon > 0$ be given, and choose l sufficiently large such that $||\psi_{i,j}^k - \psi_{i,j}^l||_2 < \epsilon, \quad \forall k, l \geq L$,
$\implies ||\psi_{i,j}^k - \psi_{i,j}^{l_n}||_2 < \epsilon, \quad \forall k, l_n \geq L$,
$\implies [\int |\psi_{i,j}^k - \psi_{i,j}^{l_n}|^2 dx] < \epsilon^2$ (using Fatous-Lemma),
$\int |\psi - \psi_{i,j}^k|^2 dx = \int \lim\limits_{k\to\infty} |\psi_{i,j}^{n_k} - \psi_{i,j}^k|^2 dx < \epsilon^2 < \infty$.

Thus, $\psi - \psi_{i,j}^k \in L_p(\mathbb{R})$ and $\psi = \psi - \psi_{i,j}^k + \psi_{i,j}^k \in L_p(\mathbb{R})$ and $\lim\limits_{n\to\infty} ||\psi - \psi_{i,j}^k||_2 = 0$.

Thus ψ is the limit in $L_2(\mathbb{R})$ of sequence $\{\psi_{i,j}^k\}$. Therefore $L_p(\mathbb{R})$ is complete. □

Theorem 3.2. *Let us assume that* $f(x) = \frac{d^n u(x)}{dx^n} \in L^2(\mathbb{R})$ *is a continuous function on [0,1] and its first derivative is bounded* $\forall x \in [0,1]$, $n \geq 2$. *Then, the Haar wavelet method will converge based on the approach proposed in [34, 35]. i.e.,* $|E_M|$ *vanishes as J goes to infinity. The convergence is of order two [33] as follows,* $||E_M||_2 = O\left[\left(\frac{1}{2^{J+1}}\right)^2\right]$.

Solution at collocation points: Let μ be a set of all measurable collocation points. Let $\{C_i\}$ be the sequence of collocation points and $\{f_i\}$ be the sequence of functional values at $\{C_i\}$ that satisfies the given system of differential equations. Here f is a function from $\mathbb{Z}^+$ to $\mathbb{R}$ defined by $f(i) = f_i$. Then

$$f(x) = \sum_{i=1}^{\infty} f(i),$$

where $f(x)$ is an exact solution of a given system of differential equations.

4. Method of solution

4.1. For integer order diabetes model

Consider the general form of the n-system of differential equations as follows:

$$\left.\begin{aligned} z_1'(t) &= f_1(t, z_1(t), ..., z_n(t)), \\ z_2'(t) &= f_2(t, z_1(t), ..., z_n(t)), \\ &\vdots \\ z_n'(t) &= f_n(t, z_1(t), ..., z_n(t)), \end{aligned}\right\} \tag{4.1}$$

with initial conditions $y_s(0)=\alpha_k$, where $s = 1, ..., n$. To determine the HWCM of the above system, we determine the collocation points as

$$t_s = 0.5\,(\tilde{t_{s-1}} + \tilde{t_s}), \qquad s = 1, ..., 2M,$$

where,

$$\tilde{t_s} = a + s\Delta t, \qquad s = 0, 1, ..., 2M.$$

Now the HWCM approximation of (4.1) can be expressed as

$$z_k'(t) = \sum_{i=1}^{2M} b_i^k h_i(t). \tag{4.2}$$

Integrating (4.2) concerning t from 0 to t, we get

$$z_k(t) = z_k(0) + \sum_{1=1}^{2M} b_i^k P_{1,i}(t),$$

$$z_k(t) = \alpha_k + \sum_{1=1}^{2M} b_i^k P_{1,i}(t). \tag{4.3}$$

$P_{1,i}$ is the first OMI. The model reduces to a nonlinear algebraic equations system by replacing the equations (4.2) and (4.3) in (4.1) and replacing t by t_s,

$$\left.\begin{aligned} &F_1(b_1^1, b_2^1, ..., b_{2M}^1, b_1^2, b_2^2, ..., b_{2M}^2, ..., b_1^n, b_2^n, ..., b_{2M}^n) = 0,\\ &F_2(b_1^1, b_2^1, ..., b_{2M}^1, b_1^2, b_2^2, ..., b_{2M}^2, ..., b_1^n, b_2^n, ..., b_{2M}^n) = 0,\\ &\qquad\vdots\\ &F_n(b_1^1, b_2^1, ..., b_{2M}^1, b_1^2, b_2^2, ..., b_{2M}^2, ..., b_1^n, b_2^n, ..., b_{2M}^n) = 0. \end{aligned}\right\} \tag{4.4}$$

To determine the values of the Haar coefficients b_i^k, the Newton-Raphson method is taken into consideration. If b_i^k is the initial guess of the root and the slope intercept point is b_{i+1}^k, (4.4) can be expressed using Taylor series expansion as follows:

$$F_{1,i+1} = F_{1,i} + (b_{1,i+1}^k - b_{1,i}^k)\frac{\partial F_{1,i}}{\partial b_1^k} + (b_{2,i+1}^k - b_{2,i}^k)\frac{\partial F_{1,i}}{\partial b_2^k} +, ..., +(b_{2M,i+1}^k - b_{2M,i}^k)\frac{\partial F_{1,i}}{\partial b_{2M}^k}, \tag{4.5}$$

where, k=1,...,n. $F_2, F_3, ..., F_n$ are expanded similarly using the Taylor series, and generalizing for n equations, we get

$$\begin{aligned} &\frac{\partial F_{k,i}}{\partial b_1^k} b_{1,i+1}^k + \frac{\partial F_{k,i}}{\partial b_2^k} b_{2,i+1}^k +, ..., + \frac{\partial F_{k,i}}{\partial b_{2M}^k} b_{2M,i+1}^k \\ &= -F_{k,i} + b_{1,i}^k \frac{\partial F_{k,i}}{\partial b_1^k} + b_{2,i}^k \frac{\partial F_{k,i}}{\partial b_2^k} +, ..., + b_{2M,i}^k \frac{\partial F_{k,i}}{\partial b_{2M}^k}. \end{aligned} \tag{4.6}$$

The function at the current value (i) or at the next value $(i+1)$ is indicated by the second subscript, and the first subscript k depicts the equations in (4.4). Matrix notation for (4.6) is as follows:

$$[J][b_{i+1}^k] = -[F] + [J][b_i^k], \tag{4.7}$$

where the partial derivatives evaluated at i are written as the Jacobian matrix consisting of partial derivatives:

$$[J] = \begin{bmatrix} \frac{\partial F_{1,i}}{\partial b_1^k} & \frac{\partial F_{1,i}}{\partial b_2^k} & \cdots & \frac{\partial F_{1,i}}{\partial b_{2M}^k} \\ \frac{\partial F_{2,i}}{\partial b_1^k} & \frac{\partial F_{2,i}}{\partial b_2^k} & \cdots & \frac{\partial F_{2,i}}{\partial b_{2M}^k} \\ \vdots & & \cdots & \vdots \\ \frac{\partial F_{n,i}}{\partial b_1^k} & \frac{\partial F_{n,i}}{\partial b_2^k} & \cdots & \frac{\partial F_{n,i}}{\partial b_{2M}^k} \end{bmatrix}.$$

The final and initial values are expressed in vector form as:

$$[b_i^k]^T = \begin{bmatrix} b_{1,i}^k & b_{2,i}^k & \cdots & b_{2M,i}^k \end{bmatrix}, \ [b_{i+1}^k]^T = \begin{bmatrix} b_{1,i+1}^k & b_{2,i+1}^k & \cdots & b_{n,i+1}^k \end{bmatrix},$$
$$\text{and } [F]^T = \begin{bmatrix} F_{1,i} & F_{2,i} & \cdots & F_{n,i} \end{bmatrix}.$$

The inverse of the Jacobian is multiplied to (4.7)

$$[b_{i+1}^k] = [b_i^k] - [J]^{-1}[F]. \tag{4.8}$$

We obtain the Haar wavelet coefficients $b_i^k s$ using (4.8). We get the intended solution of the model (4.1) by using $b_i^k s$ in equation (4.3).

4.2. For the fractional order diabetes model

Consider the general form of the system of FDEs,

$$\left.\begin{aligned} D^{\alpha}z_1(t) &= f_1(x, z_1(t), ..., z_n(t)),\\ D^{\alpha}z_2(t) &= f_2(x, z_1(t), ..., z_n(t)),\\ &\vdots\\ D^{\alpha}z_n(t) &= f_n(x, z_1(t), ..., z_n(t)), \end{aligned}\right\} \tag{4.9}$$

with initial conditions $z_s(t) = \beta_k, s = 1, 2, ..., n.$ The following is the HWCM approximation:

$$\frac{dz_k(t)}{dt} = \sum_{i=1}^{m} a_i^k h_m(t). \tag{4.10}$$

Integrating the above equation concerning to $'t'$ from 0 to t, we get

$$z_k(t) = \beta_k + \sum_{i=1}^{m} a_i^k Q^1 h_m(t), \qquad where, 1 \le k \le n, \tag{4.11}$$

where, $Q^1 H_m(t)$ is the 1^{st} order OMI. Fractionally differentiating (4.11) with respect to t of order α, where $\alpha \in (0, 1)$:

$$\frac{d^{\alpha}z_k(t)}{dt^{\alpha}} = \frac{d^{\alpha}}{dt^{\alpha}}(\beta_k) + \sum_{i=1}^{m} a_i^k Q^{1-\alpha} H_m(t). \tag{4.12}$$

Replacing t with the collocation points t_l provided in Section 2 and, substituting (4.10), (4.11), and (4.12) into (4.9), (4.9) reduces to nonlinear algebraic equations system as follows:

$$\left.\begin{aligned} &F_1(b_1^1, b_2^1, ..., b_m^1, b_1^2, b_2^2, ..., b_m^2, ..., b_1^n, b_2^n, ..., b_m^n) = 0,\\ &F_2(b_1^1, b_2^1, ..., b_m^1, b_1^2, b_2^2, ..., b_m^2, ..., b_1^n, b_2^n, ..., b_m^n) = 0,\\ &\qquad\vdots\\ &F_n(b_1^1, b_2^1, ..., b_m^1, b_1^2, b_2^2, ..., b_m^2, ..., b_1^n, b_2^n, ..., b_m^n) = 0. \end{aligned}\right\} \tag{4.13}$$

To determine the values of the Haar coefficients b_i^k's, the Newton-Raphson method is taken into consideration as follows: If b_i^k is the initial guess of the root and the slope intercept point is b_{i+1}^k, (4.13) can be expressed using Taylor series expansion as

$$F_{1,i+1} = F_{1,i} + (b_{1,i+1}^k - b_{1,i}^k)\frac{\partial F_{1,i}}{\partial b_1^k} + (b_{2,i+1}^k - b_{2,i}^k)\frac{\partial F_{1,i}}{\partial b_2^k} +, ..., +(b_{m,i+1}^k - b_{m,i}^k)\frac{\partial F_{1,i}}{\partial b_m^k}, \tag{4.14}$$

where k=1,...,n. Employing the Taylor series expansion similarly for $F_2, ..., F_n$ and generalizing for n equations, we get

$$\begin{aligned} &\frac{\partial F_{k,i}}{\partial b_1^k} b_{1,i+1}^k + \frac{\partial F_{k,i}}{\partial b_2^k} b_{2,i+1}^k +, ..., + \frac{\partial F_{k,i}}{\partial b_m^k} b_{m,i+1}^k\\ &= - F_{k,i} + b_{1,i}^k \frac{\partial F_{k,i}}{\partial b_1^k} + b_{2,i}^k \frac{\partial F_{k,i}}{\partial b_2^k} +, ..., + b_{m,i}^k \frac{\partial F_{k,i}}{\partial b_m^k}. \end{aligned} \tag{4.15}$$

The function at the current value (i) or at the next value $(i+1)$ is indicated by the second subscript, and the first subscript k depicts the equations in (4.13). Matrix notation for (4.15) is as follows:

$$[J][b_{i+1}^k] = -[F] + [J][b_i^k], \tag{4.16}$$

where the partial derivatives evaluated at i are written as the Jacobian matrix consisting of partial derivatives:

$$[J] = \begin{bmatrix} \frac{\partial F_{1,i}}{\partial b_1^k} & \frac{\partial F_{1,i}}{\partial b_2^k} & \cdots & \frac{\partial F_{1,i}}{\partial b_m^k} \\ \frac{\partial F_{2,i}}{\partial b_1^k} & \frac{\partial F_{2,i}}{\partial b_2^k} & \cdots & \frac{\partial F_{2,i}}{\partial b_m^k} \\ \vdots & & \cdots & \vdots \\ \frac{\partial F_{n,i}}{\partial b_1^k} & \frac{\partial F_{n,i}}{\partial b_2^k} & \cdots & \frac{\partial F_{n,i}}{\partial b_m^k} \end{bmatrix}.$$

The initial and final values are expressed in vector form as:

$$[b_i^k]^T = \begin{bmatrix} b_{1,i}^k & b_{2,i}^k & \cdots & b_{m,i}^k \end{bmatrix}, \quad [b_{i+1}^k]^T = \begin{bmatrix} b_{1,i+1}^k & b_{2,i+1}^k & \cdots & b_{n,i+1}^k \end{bmatrix},$$
$$\text{and} \quad [F]^T = \begin{bmatrix} F_{1,i} & F_{2,i} & \cdots & F_{n,i} \end{bmatrix}.$$

Multiplying the inverse of the Jacobian to (4.16)

$$[b_{i+1}^k] = [b_i^k] - [J]^{-1}[F]. \tag{4.17}$$

We obtain the Haar wavelet coefficients $b_i^k s$ using (4.17). We get the desired solution of (4.9) by using $b_i^k s$ in equation (4.11).

5. Numerical results

For the justification of the method, we add a nonlinear system of equation. The considered model is solved by HWCM and the obtained numerical results are compared with the other methods in the literature.

Example 5.1. Consider the following nonlinear system of two nonlinear FDEs:

$$\left.\begin{aligned} D^\alpha Y_1(t) &= -1002Y_1(t) + 1000Y_2^2(t), \\ D^\alpha Y_2(t) &= Y_1(t) - Y_2(t)(1 + Y_2(t)), \end{aligned}\right\}$$

subject to the initial condition: $Y_1(0) = 1, Y_2(0) = 1$. The exact solutions to the system when $\alpha_1 = \alpha_2 = 1$ are $Y_1(t) = e^(-2t)$ and $Y_2(t) = e^t$. The Haar wavelet collocation method (HWCM) solutions shown in Tables 1-2 reveal that the proposed method solutions are reasonably close to the exact solution compared to existing methods such as Chebyshev polynomials (CMCP), multistep fractional differential transform method (MSFDTM), fractional differential transform method (MSFDTM), and ND Solver. From the tables, it is clear that the HWCM method dominates all the other techniques in obtaining the numerical approximation and yields a satisfactory result for the desired system.

Table 1. Comparison of the A. E. of the solution $Y_1(t)$ for the Example 5.1.

t	**AE of HWCM**	**AE of MSFDTM** [37]	**AE of FDTM** [37]	**AE of CWCP (N=8)** [38]
0	0	0	0	0
0.1	4.55×10^{-10}	-	-	-
0.2	3.45×10^{-10}	-	-	0.45×10^{-8}
0.3	2.61×10^{-10}	-	-	-
0.4	1.96×10^{-10}	-	-	0.61×10^{-8}
0.5	1.45×10^{-10}	1.66×10^{-15}	1.21×10^{-3}	-
0.6	1.07×10^{-10}	-	-	0.10×10^{-8}
0.7	7.80×10^{-10}	-	-	-
0.8	5.58×10^{-10}	-	-	0.13×10^{-8}
0.9	3.91×10^{-10}	-	-	-
1.0	2.66×10^{-10}	-	-	0.53×10^{-7}

Table 2. Comparison of the A. E. of the solution $Y_2(t)$ for the Example 5.1.

t	**AE of HWCM**	**AE of MSFDTM** [37]	**AE of FDTM** [37]	**AE of CWCP (N=8)** [38]
0	0	0	0	0
0.1	2.52×10^{-10}	-	-	-
0.2	2.11×10^{-10}	-	-	0.14×10^{-10}
0.3	1.76×10^{-10}	-	-	-
0.4	1.46×10^{-10}	-	-	0.21×10^{-10}
0.5	1.20×10^{-10}	9.64×10^{-16}	2.02×10^{-5}	-
0.6	9.81×10^{-10}	-	-	0.22×10^{-10}
0.7	7.89×10^{-10}	-	-	-
0.8	6.24×10^{-10}	-	-	0.18×10^{-10}
0.9	4.84×10^{-10}	-	-	-
1.0	3.64×10^{-10}	8.54×10^{-16}	1.21×10^{-3}	0.20×10^{-10}

Now, we apply the HWCM to solve the diabetes model represented in (1.1) and (1.2). Here, the diabetes mellitus model is solved using the HWCM with the help of the operational matrix provided in Section 2. The following initial conditions and physical parameter values are considered to solve this model $\mathcal{S}(0) = 400$, $\mathcal{X}(0) = 10$, $\mathcal{I}(0) = 5$, $\mathcal{R}(0) = 3.5$, $\gamma = 1, \rho = 0.13869, \chi = 0.06654, \mu = 0.09281, \varepsilon\nu = 0.88187$, and $\eta = 0.0009$. Tables3-6 and Figures 1-4 display the HWCM solutions obtained for the value of $\alpha = 1$ (integer order), demonstrating that the suggested method solutions are comparatively close to the ND Solve results when compared to the RK4 method. Absolute errors (AE) of the developed approach with the ND Solve solution are tabulated in Tables 3-6. Numerical approximations obtained by the developed technique (HWCM) and RK4 methods are compared with the NDSolve solution (since the present model has no exact solution). Utilizing the projected HWCM yields smaller errors than utilizing other existing methods. Tables 7-10 list the model's numerical approximation at various values of α. Figures 5-8 show the graphical representation of the solution at $\alpha = 0.4, 0.6, 0.8$, respectively. Therefore, based on graphical data, we may conclude that the model depends significantly on the order of fractional derivatives, which produces more biologically realistic outcomes. Additionally, we conclude that, compared to the analogous integer order Diabetes mellitus model, the suggested model under Caputo fractional order derivative offers more prosperous and more flexible outcomes.

Table 3. Numerical comparison of the solution $\mathcal{S}(t)$ with different methods

t	**ND Solver solution**	**HWCM solution**	**RK4 solution**	**AE of HWCM with ND Solver**	**AE of RK4 with ND Solver**
0	400.0000000000	400.000000000	400.0000000000	0	0
0.1	394.5220594943	394.5220596531677	394.5220594012	1.58802×10^{-7}	9.32918×10^{-7}
0.2	389.1147104219	389.114710421998	389.1147102819	1.46486×10^{-7}	1.40026×10^{-7}
0.3	383.7775674332	383.7775674332405	383.7775672283	1.10397×10^{-7}	2.04872×10^{-7}
0.4	378.5102032063	378.510203206327	378.5102029785	1.11342×10^{-7}	2.27583×10^{-7}
0.5	373.3121524604	373.3121524604941	373.3121522332	1.30765×10^{-7}	2.27235×10^{-7}
0.6	368.1829154486	368.1829154486643	368.1829152245	1.49108×10^{-7}	2.23867×10^{-7}
0.7	363.1219613160	363.121961316041	363.1219610625	1.30799×10^{-7}	2.53493×10^{-7}
0.8	358.1287311204	358.12873112048266	358.1287308584	1.30345×10^{-7}	2.62009×10^{-7}
0.9	353.2026409085	353.202640908549	353.2026406469	1.35951×10^{-7}	2.61582×10^{-7}
1.0	348.3430843722	348.3430843722583	348.3430841079	1.35814×10^{-7}	2.64356×10^{-7}

Effect of deaths in a given time range (ρ): With variation in deaths in a given time range (ρ) Figures 9-12 represent the changes of $\mathcal{S}(t), \mathcal{X}(t), \mathcal{I}(t)$, and $\mathcal{R}(t)$. With the increase in the deaths in a given time range, the number of susceptible individuals $\mathcal{S}(t)$, the carrier infectious individuals $\mathcal{X}(t)$, the infectious individuals $\mathcal{I}(t)$, and the recovered individuals $\mathcal{R}(t)$ decrease simultaneously.

Effect of rate of transmission from susceptible to exposed individuals (η): With variation in the rate of transmission from susceptible to exposed individuals (η), Figures 13-16 represent the changes of $\mathcal{S}(t), \mathcal{X}(t), \mathcal{I}(t)$, and $\mathcal{R}(t)$. With the increase in the rate of transmission from susceptible to exposed individuals, the number of susceptible individuals $\mathcal{S}(t)$ decreases, while the number of carrier infec-

Table 4. Numerical comparison of the solution $\mathcal{X}(t)$ with different methods

t	**ND Solver solution**	**HWCM solution**	**RK4 solution**	**AE of HWCM with ND Solver**	**AE of RK4 with ND Solver**
0	10.000000000	10.000000000	10.00000000	0	0
0.1	9.2331814585	9.233181517259	9.233181626	5.87169×10^{-8}	1.67969×10^{-6}
0.2	8.5210002974	8.521000384504	8.521000742	8.70407×10^{-8}	4.44826×10^{-6}
0.3	7.8599837500	7.859983961390	7.859984535	2.11386×10^{-7}	7.85971×10^{-6}
0.4	7.2468363181	7.246836555395	7.246837317	2.37241×10^{-7}	9.99438×10^{-6}
0.5	6.6784353027	6.6784354422955	6.6784363651	1.3957×10^{-7}	1.06261×10^{-6}
0.6	6.1518261175	6.15182614731	6.1518272061	2.97256×10^{-8}	1.08914×10^{-6}
0.7	5.6642171533	5.6642172779068	5.6642184511	1.24526×10^{-7}	1.29803×10^{-6}
0.8	5.2129748960	5.2129750110	5.2129762783	1.14989×10^{-7}	1.38233×10^{-6}
0.9	4.7956172947	4.79561732503	4.7956186673	3.02624×10^{-8}	1.37311×10^{-6}
1.0	4.4098080523	4.4098080544931	4.4098094563	2.11487×10^{-9}	1.40396×10^{-6}

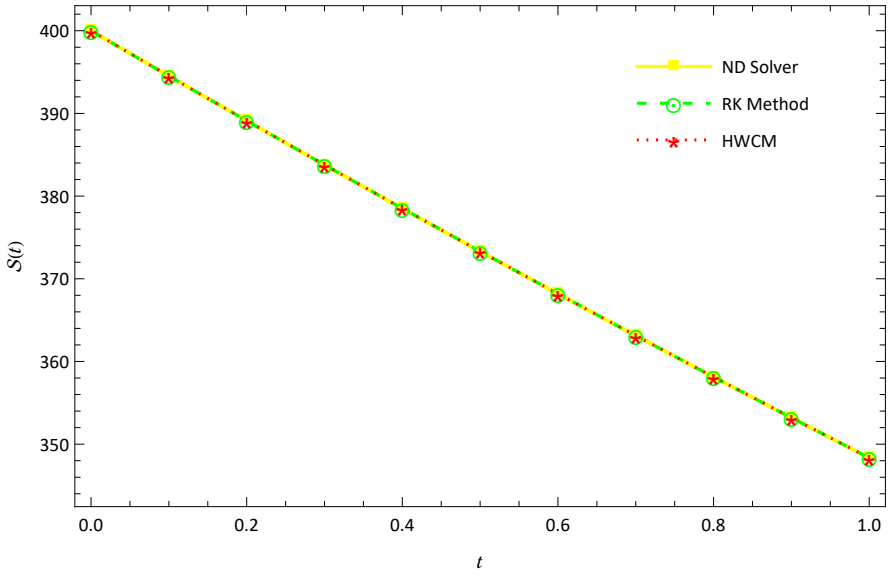

Figure 1. Graphical comparison of HWCM, ND Solver, RK Method solution for $\mathcal{S}(t)$

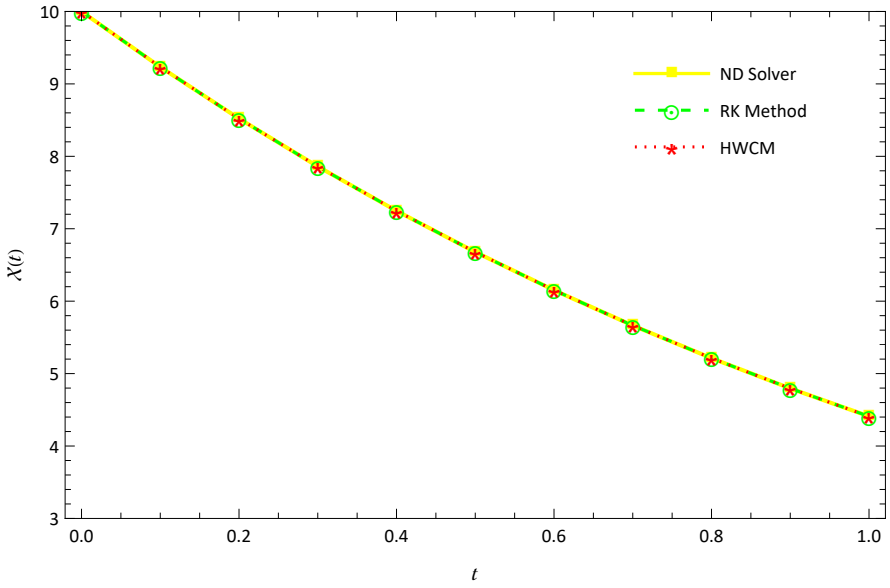

Figure 2. Graphical comparison of HWCM, ND Solver, RK Method solution for $\mathcal{X}(t)$

Table 5. Numerical comparison of the solution $\mathcal{I}(t)$ with different methods

t	**ND Solver solution**	**HWCM solution**	**RK4 solution**	**AE of HWCM with ND Solver**	**AE of RK4 with ND Solver**
0	5.0000000000	5.0000000000	5.0000000000	0	0
0.1	5.7373208704	5.737320813563	5.7373206824	5.69086×10^{-8}	1.88048×10^{-7}
0.2	6.395148632	6.39514849758	6.3951480295	1.3497×10^{-7}	6.0302×10^{-7}
0.3	6.9797138830	6.97971343543	6.9797126768	4.47661×10^{-7}	1.20622×10^{-6}
0.4	7.4968248020	7.49682434776	7.4968233408	4.5433×10^{-7}	1.46121×10^{-6}
0.5	7.9518921087	7.9518918900	7.9518906730	2.18735×10^{-7}	1.43572×10^{-6}
0.6	8.3499516074	8.34995163364	8.3499502410	2.61612×10^{-8}	1.3664×10^{-6}
0.7	8.6956863102	8.69568614843	8.6956846113	1.61798×10^{-7}	1.69884×10^{-6}
0.8	8.9934463025	8.99344616908	8.9934445155	1.33488×10^{-7}	1.78707×10^{-6}
0.9	9.2472708237	9.2472708390	9.2472690932	1.52779×10^{-8}	1.72987×10^{-6}
1.0	9.4609069625	9.46090703131	9.4609052168	6.87247×10^{-8}	1.74573×10^{-6}

Table 6. Numerical comparison of the solution $\mathcal{R}(t)$ with different methods

t	**ND Solver solution**	**HWCM solution**	**RK4 solution**	**AE of HWCM with ND Solver**	**AE of RK4 with ND Solver**
0	3.5000000000	3.5000000000	3.5000000000	0	0
0.1	3.5321294064	3.532129401867	3.5321293783	4.59449×10^{-9}	2.80726×10^{-8}
0.2	3.5548929220	3.554892906512	3.5548928361	1.55809×10^{-8}	8.59567×10^{-8}
0.3	3.5691223638	3.569122304680	3.5691221939	5.91491×10^{-8}	1.69918×10^{-7}
0.4	3.5755909308	3.57559087092	3.5755907256	5.99059×10^{-8}	2.0516×10^{-7}
0.5	3.5750167447	3.57501671743	3.5750165430	2.73348×10^{-8}	2.01723×10^{-7}
0.6	3.5680660425	3.568066048955	3.5680658502	6.42504×10^{-9}	1.92264×10^{-7}
0.7	3.5553563050	3.5553562855	3.5553560668	1.9561×10^{-8}	2.38201×10^{-7}
0.8	3.5374590668	3.53745905110	3.5374588164	1.57205×10^{-8}	2.50407×10^{-7}
0.9	3.5149030235	3.5149030280	3.5149027808	4.53021×10^{-9}	2.42712×10^{-7}
1.0	3.4881766660	3.48817667783	3.4881764211	1.17487×10^{-8}	2.44941×10^{-7}

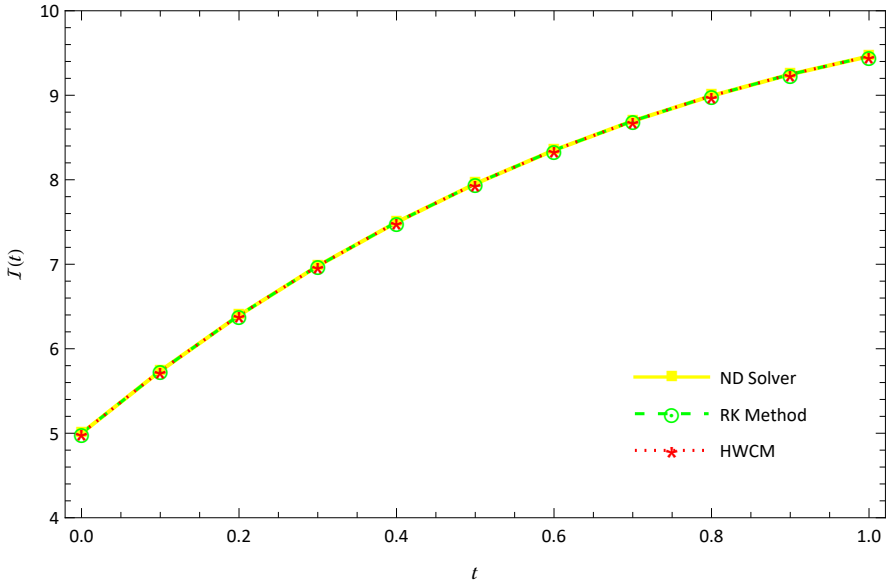

Figure 3. Graphical comparison of HWCM, ND Solver, RK Method solution for $\mathcal{I}(t)$

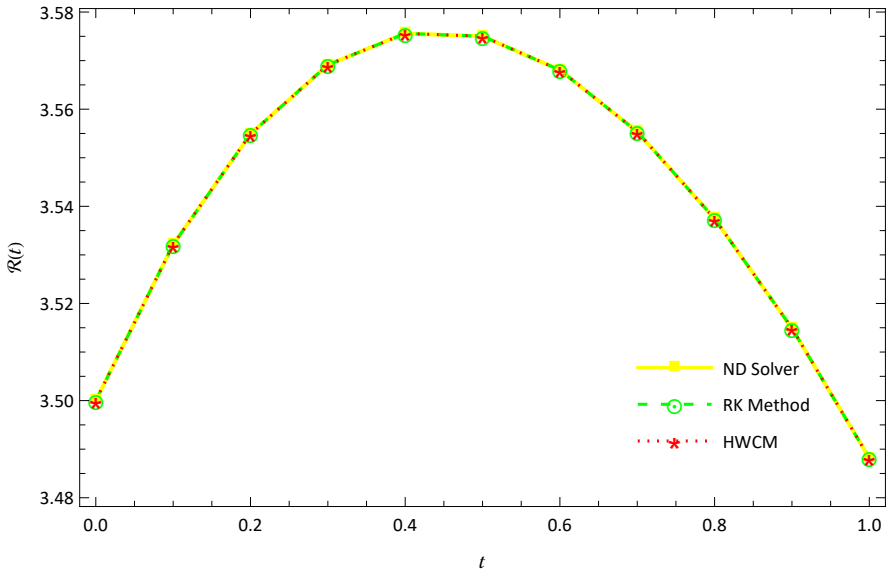

Figure 4. Graphical comparison of HWCM, ND Solver, RK Method solution for $\mathcal{R}(t)$

Table 7. HWCM solution at different values of α for $\mathcal{S}(t)$

t	**Haar wavelet solution at**			
	α**=0.2**	α**=0.4**	α**=0.6**	α**=0.8**
0	400.0000000000	400.0000000000	400.0000000000	400.000000000
0.1	362.3758200103116	375.1265727302	384.7773900061	390.9155198730
0.2	360.145639661270	369.4584242616	377.4986616869	384.1674465410
0.3	358.077181743496	364.4451286769	371.5555971929	378.2199708623
0.4	355.3901629947003	360.4111689505	366.5022377000	372.7718148950
0.5	353.2861472966467	357.0598694565	362.0271108269	367.6825680827
0.6	351.7776911928322	354.1381736810	357.9702426456	362.8743735243
0.7	350.5202763928997	351.5290052446	354.2371063761	358.2976238019
0.8	349.3600927856298	349.1635088432	350.7650367878	353.9178700539
0.9	348.292060883805	346.9938507527	347.5096676164	349.7097311086
1.0	347.2688940828827	344.9852075280	344.4379956306	345.6536212698

Table 8. HWCM solution at different values of α for $\mathcal{X}(t)$

t	**Haar wavelet solution at**			
	α**=0.2**	α**=0.4**	α**=0.6**	α**=0.8**
0	10.000000000	10.000000000	10.000000000	10.0000000000
0.1	6.0590007912	7.0390052867	8.0257429329	8.7636803598
0.2	5.9383703356	6.6036403784	7.2641996533	7.9395932316
0.3	5.8685176195	6.2026447470	6.6909208617	7.2742364726
0.4	5.6750763230	5.8909678797	6.2443298674	6.7117536320
0.5	5.5052924252	5.6519308124	5.8774171060	6.2242189339
0.6	5.4064340542	5.4546704362	5.5660700074	5.7951567476
0.7	5.3411696921	5.2856087215	5.2962791500	5.4135523479
0.8	5.2770840982	5.1379472586	5.0588811336	5.0714735471
0.9	5.2114457195	5.0070856075	4.8474805281	4.7629149317
1.0	5.1285850435	4.8896623743	4.6573927722	4.4831504000

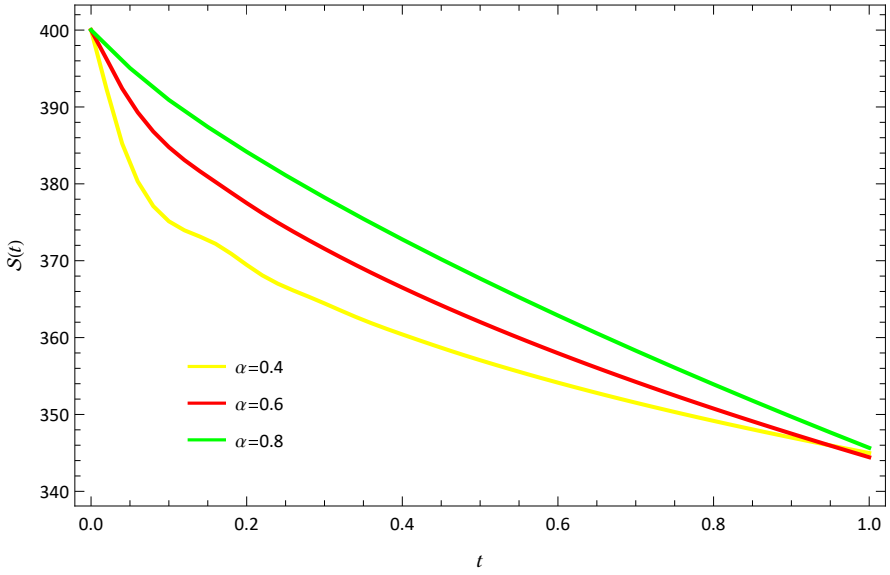

Figure 5. Graphical representation of $\mathcal{S}(t)$ with distinct values of α

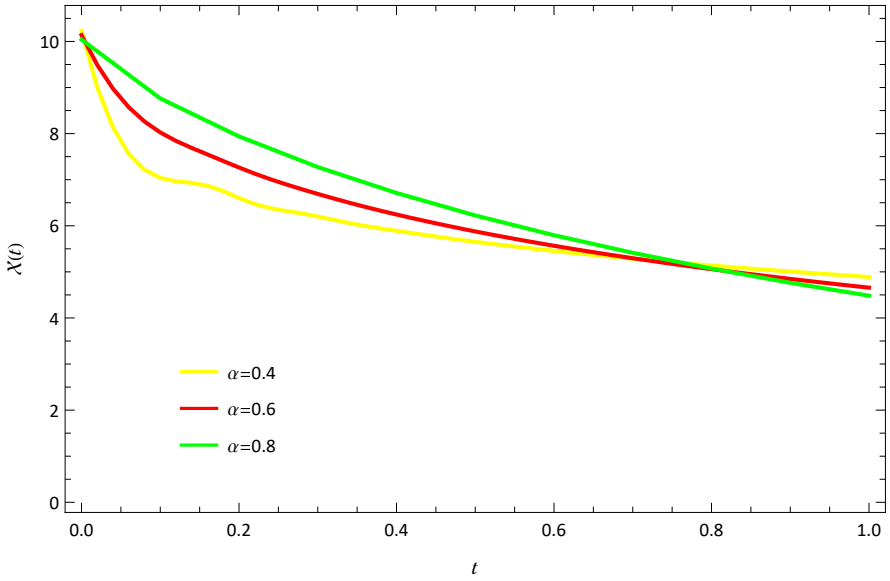

Figure 6. Graphical representation of $\mathcal{X}(t)$ with distinct values of α

Table 9. HWCM solution at different values of α for $\mathcal{I}(t)$

t	**Haar wavelet solution at**			
	α**=0.2**	α**=0.4**	α**=0.6**	α**=0.8**
0	5.0000000000	5.0000000000	5.0000000000	5.00000000000
0.1	8.0315001339	7.5415287460	6.8046097274	6.1673433136
0.2	8.0417077845	7.7565340056	7.3868445719	6.8881114857
0.3	7.9909155305	7.9749952651	7.7905223687	7.4304352920
0.4	8.0790855246	8.1357844299	8.0736471983	7.8566227604
0.5	8.1748221750	8.2407731461	8.2829727112	8.1986211279
0.6	8.2099020730	8.3167175278	8.4423439166	8.4756281132
0.7	8.2145764163	8.3748004429	8.5654195291	8.7006209222
0.8	8.2247973652	8.4198208368	8.6610271846	8.8829993546
0.9	8.2438560893	8.4549347635	8.7352516738	9.0298954265
1.0	8.2906987795	8.4824539516	8.7924916523	9.1469194137

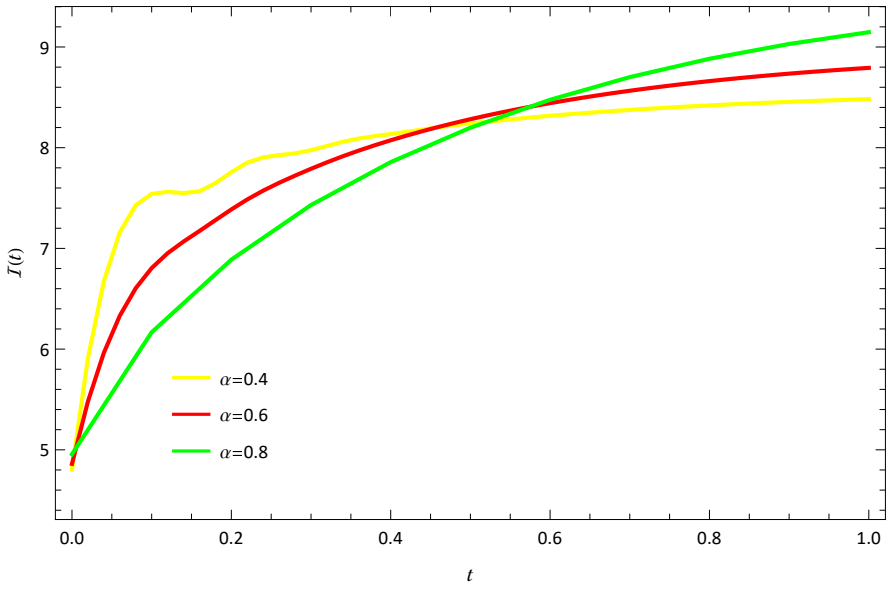

Figure 7. Graphical representation of $\mathcal{I}(t)$ with distinct values of α

Table 10. HWCM solution at different values of α for $\mathcal{R}(t)$

t	**Haar wavelet solution at**			
	α**=0.2**	α**=0.4**	α**=0.6**	α**=0.8**
0	3.5000000000	3.5000000000	3.5000000000	3.5000000000
0.1	3.4664953178	3.5438711052	3.5581752744	3.5462056677
0.2	3.4444334934	3.5087476532	3.5505477135	3.5618875723
0.3	3.4164494262	3.4814372090	3.5355441045	3.5639892219
0.4	3.3986890729	3.4578908539	3.5154528122	3.5570872622
0.5	3.3882761058	3.4349527008	3.4926776059	3.5436877691
0.6	3.3768139154	3.4131588476	3.4684237688	3.5253687994
0.7	3.3642034668	3.3926119381	3.4433428122	3.5032290817
0.8	3.3532993639	3.3731430710	3.4178344802	3.4780790308
0.9	3.3445156595	3.3546118182	3.3921586336	3.4505400510
1.0	3.3398019776	3.3369184049	3.3664908174	3.4211034271

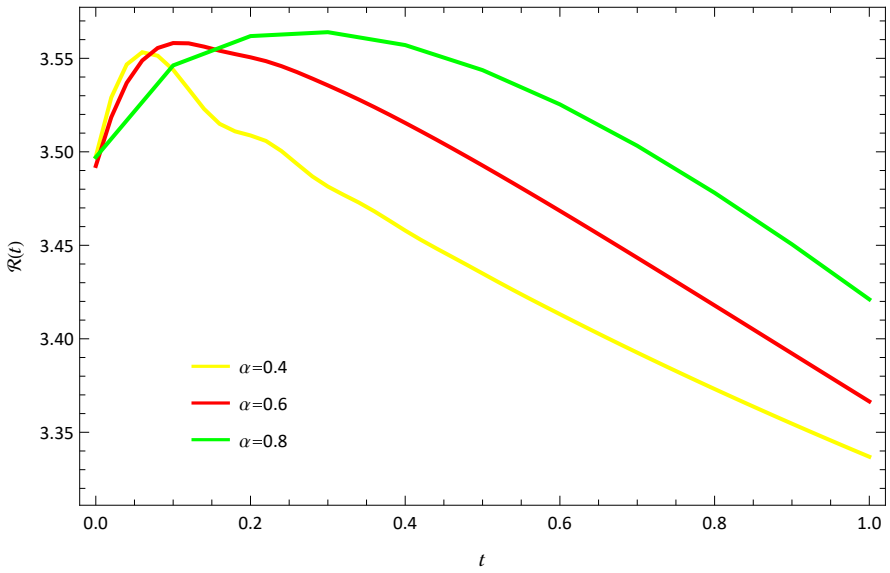

Figure 8. Graphical representation of $\mathcal{R}(t)$ with distinct values of α

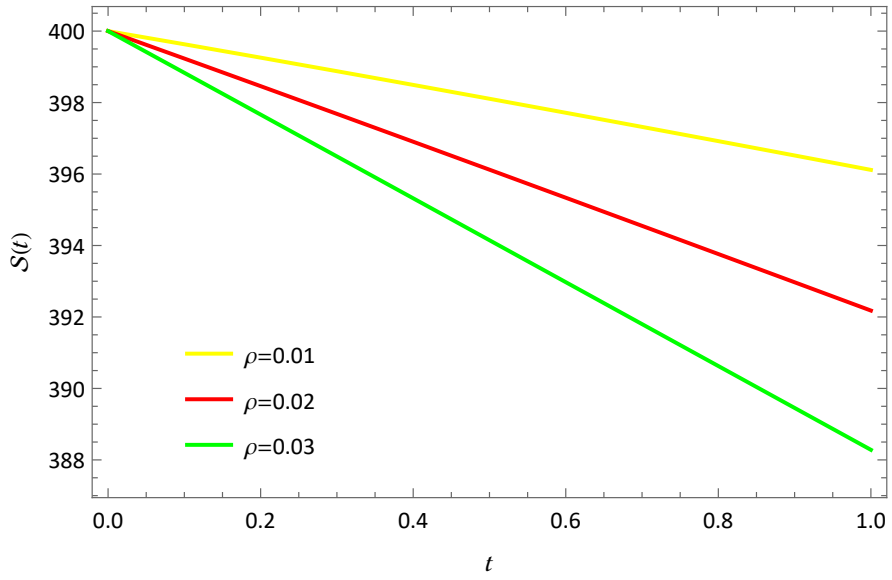

Figure 9. Graphical representation of $\mathcal{S}(t)$ for variation of ρ

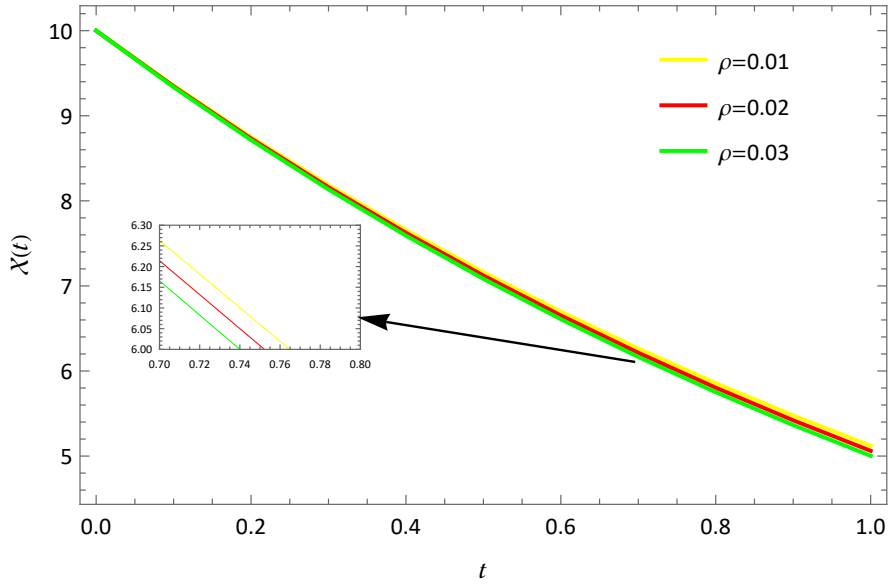

Figure 10. Graphical representation of $\mathcal{X}(t)$ for variation of ρ

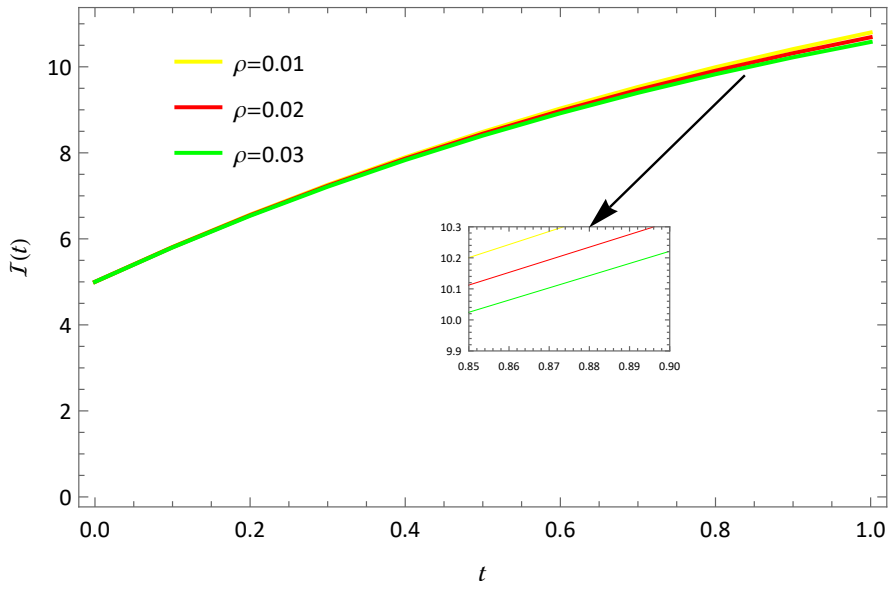

Figure 11. Graphical representation of $\mathcal{I}(t)$ for variation of ρ

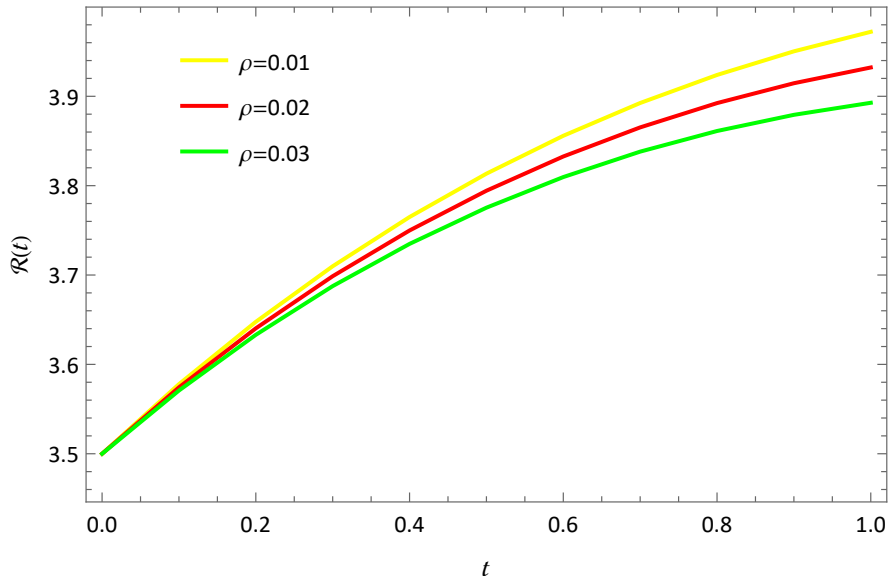

Figure 12. Graphical representation of $\mathcal{R}(t)$ for variation of ρ

tious individuals $\mathcal{X}(t)$, the infectious individuals $\mathcal{I}(t)$, and the recovered individuals $\mathcal{R}(t)$ increases simultaneously.

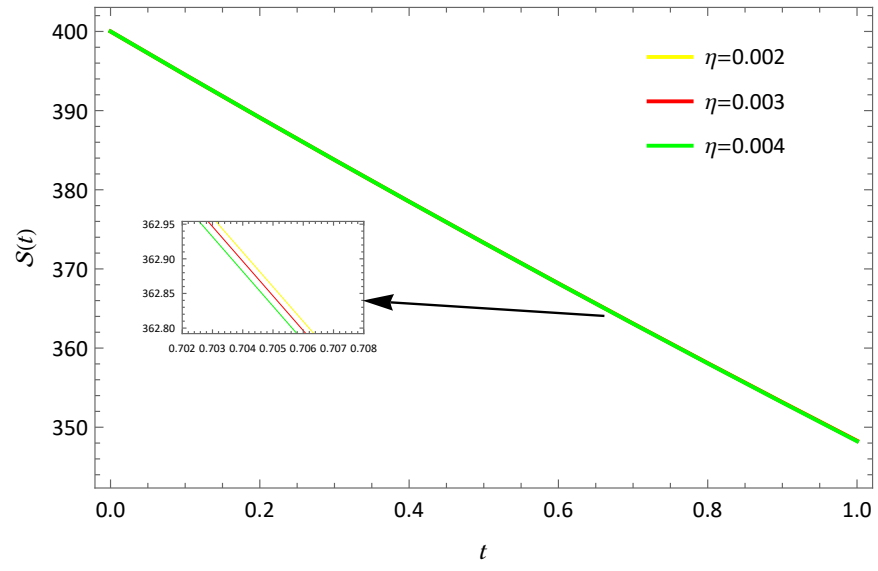

Figure 13. Graphical representation of $\mathcal{S}(t)$ for variation of η

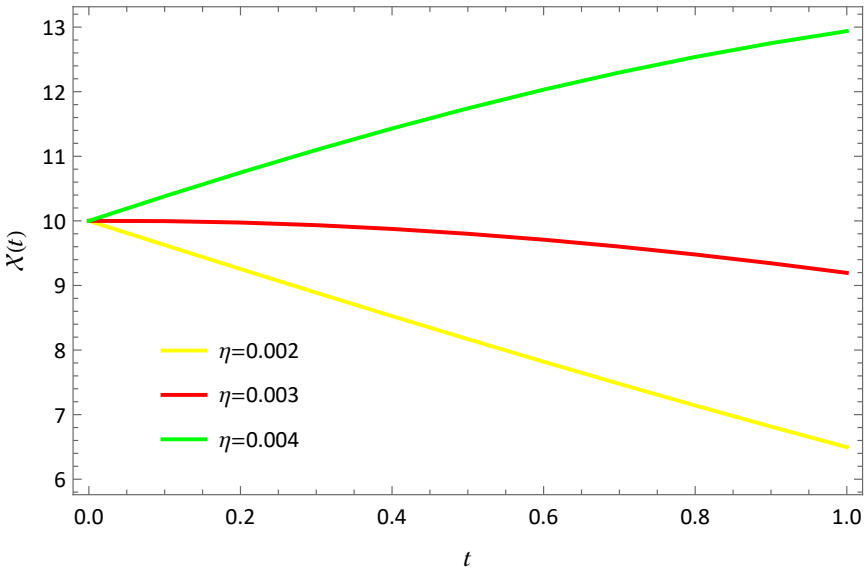

Figure 14. Graphical representation of $\mathcal{X}(t)$ for variation of η

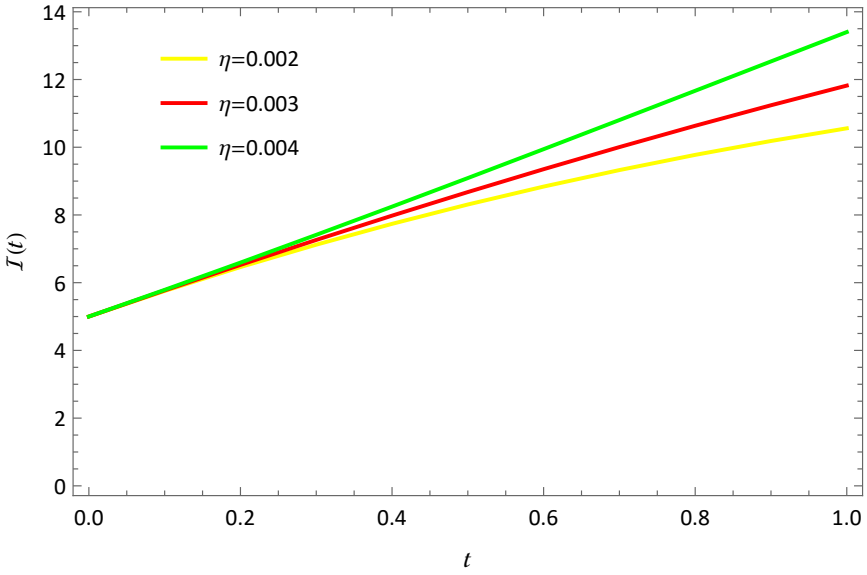

Figure 15. Graphical representation of $\mathcal{I}(t)$ for variation of η

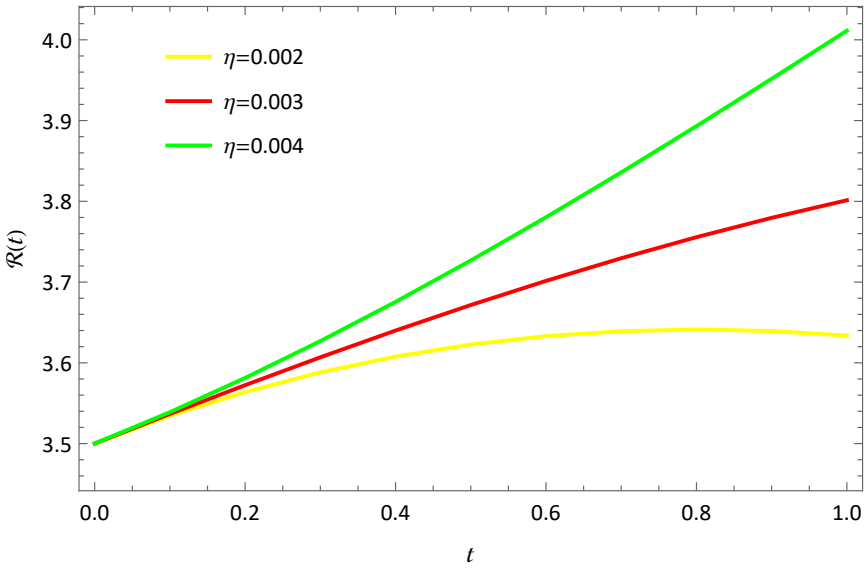

Figure 16. Graphical representation of $\mathcal{R}(t)$ for variation of η

6. Conclusion

In this study, we considered a fractional-order model of the Diabetes mellitus. The numerical solution was obtained using the Caputo fractional derivative and the HWCM. An OMI based on Haar wavelets and collocation technique was constructed to solve the model numerically. Using the abovementioned method, the mathematical models (1.1) and (1.2) were solved numerically. The HWCM more closely matches the nature and solution of the model when compared to other numerical approaches such as ND Solve and RK method, as shown in Figures 1-4 and Tables 3-6. For different values of α, the fractional order model is graphically displayed in Figures 5-8. The numerical values of the fractional order model for various values of α are displayed in Tables 7-10. This method yields results that agree with Mathematica's ND solver. Tables and figures demonstrate that the proposed method outperforms the existing numerical methods regarding precision. Numerical examples further substantiate that a small number of Haar wavelets is necessary to achieve acceptable results. Despite its ease of use, the method produced excellent results. Our belief that the technique works well for managing highly nonlinear FDEs was reinforced. We concluded that, compared to RK4, the approach is a valuable tool for obtaining the numerical approximation of the mathematical models in the form of nonlinear FDEs. The proposed techniques can be used for different mathematical models to solve them numerically and understand the geometrical interpretations of the models.

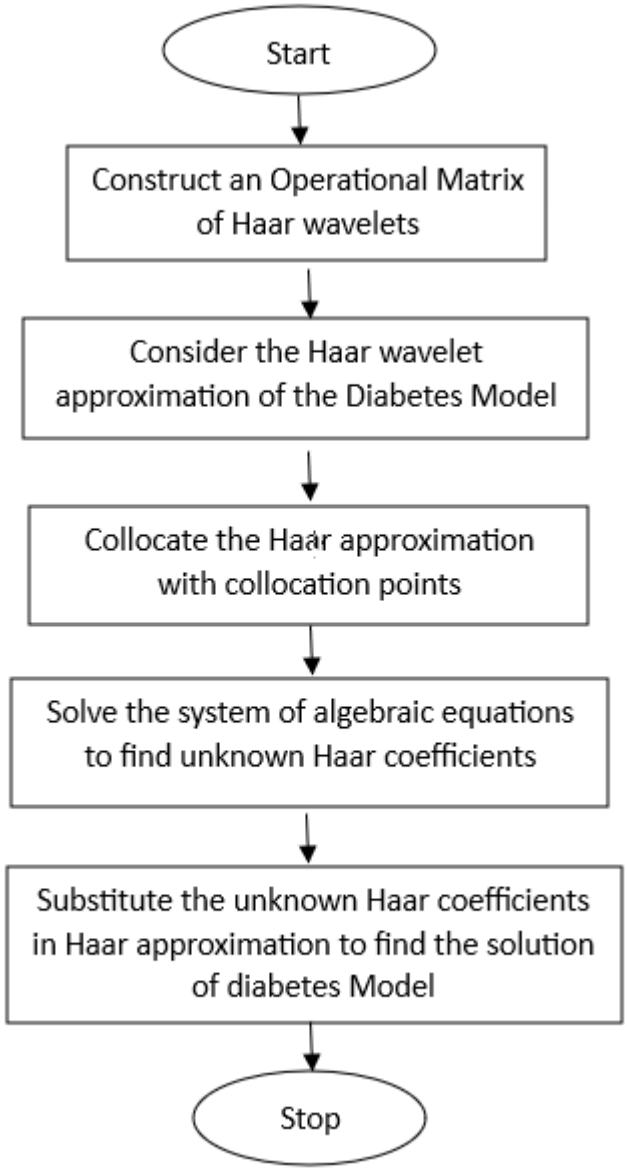

Figure 17. Flowchart of the proposed approach

Acknowledgements

The authors express his affectionate thanks to the DST-SERB, Government of India, New Delhi for the financial support under Empowerment and Equity Opportunities for Excellence in Science for 2023-2026. F.No.EEQ/2022/620 Date:07/02/2023.

Declarations:

Ethical Approval: Not applicable.

Data availability: The data supporting this study's findings are available within the article.

Conflict of Interest: Authors declare no Conflict of Interest.

References

[1] Zheng, Yan, Sylvia H. Ley, and Frank B. Hu, *Global aetiology and epidemiology of type 2 diabetes mellitus and its complications*, Nature Reviews Endocrinology 14.2 (2018), 88–98.

[2] Omame, Andrew, et al., *A fractional order control model for Diabetes and COVID-19 co-dynamics with Mittag-Leffler function*, Alexandria Engineering Journal 61.10 (2022), 7619–7635.

[3] Bonyah, Ebenezer, et al., *On the co-infection of dengue fever and Zika virus*, Optimal Control Applications and Methods 40.3 (2019), 394–421.

[4] Ahmed, Shahid, et al., *On mathematical modelling of measles disease via collocation approach*, AIMS Public Health 11.2 (2024), 628–653.

[5] Zhao, Jin-Qiang, et al., *A mathematical model for the coinfection of Buruli ulcer and cholera*, Results in Physics 29 (2021), 104746.

[6] Omame, A., et al., *A co-infection model for HPV and syphilis with optimal control and cost-effectiveness analysis*, International Journal of Biomathematics 14.07 (2021), 2150050.

[7] Kharroubi, Akram T., and Hisham M. Darwish, *Diabetes mellitus: The epidemic of the century*, World journal of diabetes 6.6 (2015), 850.

[8] Yadav, Pooja, et al., *Fractional-order modelling and analysis of diabetes mellitus: Utilizing the Atangana-Baleanu Caputo (ABC) operator*, Alexandria Engineering Journal 81 (2023), 200–209.

[9] Saleem, Muhammad Umer, et al., *A Caputo Fabrizio fractional order model for control of glucose in insulin therapies for diabetes*, Ain Shams Engineering Journal 11.4 (2020), 1309–1316.

[10] Srivastava, Hari M., Ravi Shanker Dubey, and Monika Jain, *A study of the fractional-order mathematical model of diabetes and its resulting complications*, Mathematical Methods in the Applied Sciences 42.13 (2019), 4570–4583.

[11] Mollah, Saddam, Santosh Biswas, and Subhas Khajanchi, *Impact of the awareness program on diabetes mellitus described by fractional-order model solving by homotopy analysis method*, Ricerche di Matematica (2022), 1–26.

[12] Narayanan, Govindasamy, et al., *Stability analysis for Nabla discrete fractional-order of Glucose-Insulin Regulatory System on diabetes mellitus with Mittag-Leffler kernel*, Biomedical Signal Processing and Control 80 (2023), 104295.

[13] Goharimanesh, Masoud, Ali Lashkaripour, and Ali Abouei Mehrizi, *Fractional order PID controller for diabetes patients*, Journal of Computational Applied Mechanics 46.1 (2015), 69–76.

[14] Narayanan, G., Ali, M. S., Rajchakit, G., Jirawattanapanit, A., & Priya, B, *Stability analysis for Nabla discrete fractional-order of Glucose-Insulin Regulatory System on diabetes mellitus with Mittag-Leffler kernel*, Biomedical Signal Processing and Control, 80 (2023), 104295.

[15] Narayanan, G., Ali, M. S., Karthikeyan, R., Rajchakit, G., & Jirawattanapanit, A, *Novel adaptive strategies for synchronization control mechanism in nonlinear dynamic fuzzy modeling of fractional-order genetic regulatory networks*, Chaos, Solitons & Fractals, 165 (2022), 112748.

[16] Lepik, Ülo, *Numerical solution of differential equations using Haar wavelets*, Mathematics and computers in simulation 68.2 (2005), 127–143.

[17] Lepik, Ülo, *Application of the Haar wavelet transform to solving integral and differential equations*, Proceedings of the Estonian Academy of Sciences, Physics, Mathematics. Vol. 56. (2007).

[18] Kumbinarasaiah, S., and R. Yeshwanth, *A study on Chlamydia transmission in United States through the Haar wavelet technique*, Results in Control and Optimization (2024), 100396.

[19] Preetham, M. P., S. Kumbinarasaiah, and K. R. Raghunatha, *Squeezing Flow of an Electrically Conducting Casson Fluid by Hermite Wavelet Technique*, WSEAS Transactions on Fluid Mechanics 18 (2023), 221–232.

[20] Mulimani, Mallanagoud, and S. Kumbinarasaiah, *A numerical study on the nonlinear fractional Klein-Gordon equation*, Journal of Umm Al-Qura University for Applied Sciences 10.1 (2024), 178–199.

[21] Mulimani, Mallanagoud, and Kumbinarasaiah S, *Numerical solution of time-fractional telegraph equations using wavelet transform*, International Journal of Dynamics and Control (2023), 1–24.

[22] Manohara, G., and S. Kumbinarasaiah, *Numerical approximation of fractional SEIR epidemic model of measles and smoking model by using Fibonacci wavelets operational matrix approach*, Mathematics and Computers in Simulation (2024).

[23] Manohara, G., and S. Kumbinarasaiah, *Numerical solution of some stiff systems arising in chemistry via Taylor wavelet collocation method*, Journal of Mathematical Chemistry 62.1 (2024), 24–61.

[24] Chen, Qiliang, et al., *A fractional study based on the economic and environmental mathematical model*, Alexandria Engineering Journal 65 (2023), 761–770.

[25] Kumbinarasaiah, S., and R. Yeshwanth, *Haar wavelet approach to study the control of biological pest model in Tea plants*, Journal of Fractional Calculus and Nonlinear Systems 4.2 (2023), 14–30.

[26] Ahmeda, Shahid, Shah Jahana, and Kottakkaran Sooppy Nisarb, *Haar wavelet based numerical technique for the solutions of fractional advection diffusion equations*, Journal of Mathematics and Computer Science 34.3 (2024), 217–233.

[27] Yadav, Pooja, Shah Jahan, and Kottakkaran Sooppy Nisar, *Fibonacci wavelet method for time fractional convection-diffusion equations*, Mathematical Methods in the Applied Sciences 47.4 (2024), 2639–2655.

[28] Kumbinarasaiah, S., and R. Yeshwanth, *A numerical study of the evolution of smoking habit model through Haar wavelet technique*, International Journal of Dynamics and Control (2024), 1–19.

[29] Izadi, Mohammad, Pundikala Veeresha, and Waleed Adel, *The fractional-order marriage-divorce mathematical model: numerical investigations and dynamical analysis*, The European Physical Journal Plus 139.3 (2024), 205.

[30] Yadav, Pooja, Shah Jahan, and Mohammad Izadi, *Taylor wavelet quasilinearization method for solving tumor growth model of fractional order*, Results in Control and Optimization (2024), 100437.

[31] Yadav, Pooja, Shah Jahan, and Kottakkaran Sooppy Nisar, *Shifted fractional order Gegenbauer wavelets method for solving electrical circuits model of fractional order*, Ain Shams Engineering Journal 14.11 (2023), 102544.

[32] Ahmed, Shahid, et al., *Wavelets collocation method for singularly perturbed differential-difference equations arising in control system*, Results in Applied Mathematics 21 (2024), 100415.

[33] Majak, Jüri, et al., *Convergence theorem for the Haar wavelet based discretization method*, Composite Structures 126 (2015), 227–232.

[34] Chen, Chi Fan, and Chi-Huang Hsiao, *Haar wavelet method for solving lumped and distributed-parameter systems*, IEE Proceedings-Control Theory and Applications 144.1 (1997), 87–94.

[35] Hsiao, Chun-Hui, *State analysis of linear time delayed systems via Haar wavelets*, Mathematics and Computers in Simulation 44.5 (1997): 457–470.

[36] Kumbinarasaiah, S, *A novel approach for multi dimensional fractional coupled Navier-Stokes equation*, SeMA Journal 80.2 (2023): 261–282.

[37] Alkresheh, H. A., & Ismail, A. I, *Multi-step fractional differential transform method for the solution of fractional order stiff systems*, Ain Shams Engineering Journal, 12(4) (2021), 4223–4231.

[38] Ozturk, Y, *Numerical solution of systems of differential equations using operational matrix method with Chebyshev polynomials*, Journal of Taibah University for Science, 12(2) (2018), 155–162.